J Electroceram (2014) 33:221–229
DOI 10.1007/s10832-014-9954-9

Defect chemistry and transport properties of Nd-doped $Pb(Zr_xTi_{1-x})O_3$

Christoph Slouka · Lukas Andrejs · Jürgen Fleig

Received: 22 November 2013 / Accepted: 25 June 2014 / Published online: 16 July 2014

Abstract The oxygen partial pressure (pO_2) dependent conductivity of Nd^{3+} doped PZT was investigated at different temperatures in order to get information on the nature of the conducting charge carriers and on the chemical oxygen diffusion coefficient. From a positive slope close to 0.25 in log (conductivity) vs. log (pO_2) plots it is concluded that PZT with donor-type Nd^{3+} shows predominant hole conduction already at moderately high oxygen partial pressures, while under reducing conditions electron conduction prevails. This unexpected occurrence of hole conduction in a nominally donor doped system is interpreted in terms of the only partially controllable loss of lead oxide during preparation, which results in the formation of lead vacancies. Those act as acceptors at the temperatures employed in this study (560–615 °C) and turn the nominally donor doped material into a slightly acceptor doped one. From the conductivity relaxation after partial pressure changes, chemical oxygen diffusion coefficients could be extracted and values of about $6.5 \cdot 10^{-9}$ cm^2/s at 560 °C and $2 \cdot 10^{-8}$ cm^2/s at 611 °C are found in air.

Keywords Defect chemistry · PZT · Impedance spectroscopy · Chemical diffusion in solids

1 Introduction

Perovskite-type oxides are employed in many electroceramic devices. Among the most important examples are barium titanate (BTO) for positive temperature coefficient resistors and multilayer ceramic capacitors [1], strontium titanate (STO) used as oxygen sensor at high temperatures [2] and lead zirconate titanate, $Pb(Zr_xTi_{1-x})O_3$ (PZT), applied in generators, motors, ultrasonic transducers, actuators, capacitors or non-volatile memories [3, 4]. In all these devices, point defects strongly affect materials properties and thus numerous efforts have been made in order to obtain a clear understanding of the defect thermodynamics and kinetics in perovskites-type oxides. Many defect chemical relations could be established, including their dependence on oxygen partial pressure, temperature and doping. Particularly for BTO [5–9], and STO [10–14] defect chemistry is rather well understood.

Interestingly, despite many applications and good knowledge in processing, the nature, concentration and importance of defects in PZT is still partly under discussion [15–21]. Characteristic properties such as high permittivity, electromechanical coupling factor, piezoelectric strain coefficients or remanent polarization are strongly affected by the Zr:Ti ratio and can be further modified by doping, i.e. by defects (soft or hard PZT). Donor-type doping causes an enhancement of the concentration of cation vacancies (in most cases lead vacancies [22]) and thus results in a reduction of the oxygen vacancy concentration via Schottky equilibrium. In contrast, acceptor doping is a strategy for enhancing the oxygen vacancy concentration in PZT [3]. The processing parameters, such as sintering temperature or quenching procedure have also effects on the performance and this is partly attributed to point defect concentrations [23].

One might argue that little difference should exist in defect chemistry of PZT, STO and BTO. However, the volatility of PbO at higher temperatures [24, 25] leads to an additional experimental parameter in preparation of PZT and causes partly uncontrollable variations of the stoichiometry. This makes the prediction of defect concentrations problematic. Since frozen-in cation vacancies can act as kind of acceptor dopant, even effective dopant concentrations are often

C. Slouka · L. Andrejs · J. Fleig (✉)
Christian Doppler Laboratory of Ferroic Materials, Institute of Chemical Technologies and Analytics, Vienna University of Technology, Getreidemarkt 9-164/EC, 1060 Vienna, Austria
e-mail: j.fleig@tuwien.ac.at

unknown in PZT. Several studies were performed to determine the majority charge carriers at different oxygen partial pressures and temperatures [17, 18, 26, 27]. For example, undoped PZT with a composition near the morphotropic phase boundary showed pronounced hole conduction with varying conductivity in the oxygen partial pressure range of 1–10^{-4} bar [20]. A decrease of the conductivity in Nb^{5+} doped PZT when changing the atmosphere from air to nitrogen was interpreted as an indication of hole conduction [18]. Earlier measurements also suggested hole conduction from the dopant dependence of the conductivity [28–30].

However, the partial pressure dependent conductivity of nominally donor-doped PZT was not analyzed in detail yet and it is still an open question, under which conditions donor dopants successfully suppress hole conduction, as they usually do in STO and BTO. Also defect diffusion in PZT has been analyzed much less than in BTO and STO. Cation vacancies seem to be immobile up to moderate temperatures of 500 to 700 °C [25]. The main actors in diffusion processes are thus assumed to be oxygen vacancies and electrons or electron holes [18]. Chemical diffusion coefficients can be extracted from conductivity relaxation experiments after partial pressure changes [31] and such measurements were performed on a PZT buried capacitor structure [18]. This type of diffusion deals with cooperative motion of electronic and ionic charge carriers. Oxygen tracer diffusion, on the other hand, essentially monitors ionic conductivity and measurements on donor-doped PZT revealed fast oxygen ion transport along grain boundaries above 600 °C [15]. A further approach to analyze ionic defect motion in such oxides is based on impedance spectroscopy (EIS) [32, 33], which may allow the determination of ionic and electronic contributions to the conductivity when using ion blocking electrodes. This method was already applied to undoped and Nb-doped PZT near the morphotropic phase boundary [25, 26] and novel results on donor-doped PZT will be given in a forthcoming paper.

In this contribution, Nd^{3+} donor-doped PZT samples with a composition near the morphotropic phase boundary were analyzed by conductivity relaxation studies, monitored via impedance spectroscopy. Temperatures in the range of 560–615 °C allowed relaxation measurements on a reasonable time scale (up to a few days) while still largely avoiding lead oxide evaporation. Temperature and oxygen partial pressure was varied and the resulting partial pressure and time dependence of the conductivity revealed information on the charge carriers determining the conductivity and the chemical oxygen diffusion coefficients in PZT. It is shown that moderate donor doping of PZT does not necessarily suppress predominant hole conduction in air.

2 Experimental

The PZT samples (0.6 × 0.6 × 0.05 cm^3 supplied by EPCOS OHG A Group Company of TDK-EPC Corporation, Deutschlandsberg, Austria) consisted of 2 mol % Nd-doped PZT close to the morphotropic phase boundary and were sintered at 1050 °C in wet H_2/N_2 atmosphere. The dopant (Nd_2O_3) was added before calcination and homogeneity within the grains can thus be assumed. A Pb excess of 2 mol% was employed (before calcination) to take account of the high volatility of PbO. Platinum paste (Gwent Group, UK) was used to deposit electrodes on two sides of the PZT specimen and the resulting sample geometry is given in Fig. 1. Prefiring of the Pt paste was not performed in order to avoid irreversible sample changes; good adhesion was already obtained simply by heating to the measurement temperatures.

The gas composition was established via a Rod4 (Aera) control unit with different mass flow controllers (Aera) (MFC) by mixing the following gases: The O_2 partial pressure range from 1 to 10^{-5} bar was established by oxygen - nitrogen mixtures using pure O_2 or 1 % O_2 in N_2 and pure N_2 as source gases. Pure N_2 and the reduction of the total pressure by a vacuum pump were used for achieving even lower pressures at 565 °C. Humified 2.5 % H_2 in Ar was employed for a measurement under reducing conditions. At a temperature of 565 °C this corresponds to an oxygen partial pressure (pO_2) of ca. $2{\cdot}10^{-25}$ bar. The temperature was measured by a type K or S thermocouple positioned close to the sample. A N4L PSM 1735 (Numetriq) with IAI - Impedance Analysis Interface (Numetriq) was used for impedance analysis (1 MHz to 10 mHz, 0.01 to 0.1 V amplitude). The outflowing gas was analyzed by an oxygen sensor Rapidox 2100 (Cambridge Sensotec) in order to determine or verify the nominally established gas composition.

The samples were first heated to temperatures between 560 and 615 °C in ambient air. The temperature range was limited by irreversible sample changes at higher temperatures and slow kinetics at lower temperatures. After temperature stabilization within +/−0.5 °C impedance measurements were started. The impedance measurements were repeated automatically in intervals of 60 to 900 s. Before performing pO_2-dependent measurements, all virgin samples underwent a kind of first equilibration under atmospheric partial pressure until a constant conductivity was reached. After this first equilibration, oxygen partial pressure steps were applied and conductivity changes were monitored by continuous impedance measurements until a constant conductivity value was again reached.

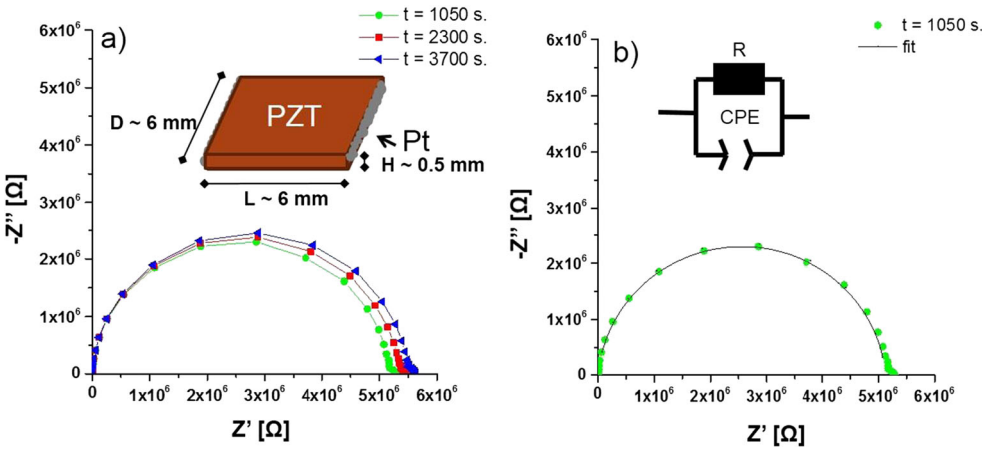

Fig. 1 Impedance spectra measured at 560 °C and sketch of the sample geometry. The spectra show the time dependence after reaching constant temperature **a** and a spectrum with a fit to the given equivalent circuit **b**

3 Results and discussion

3.1 Impedance spectra and time dependence of the conductivity

In Fig. 1 typical impedance spectra measured on the PZT samples are shown. In almost all cases, one semicircle is visible in the complex impedance plane irrespective of relaxation state and oxygen partial pressure. The small shoulder often found at low frequencies might be caused by non-ohmic contacts (Schottky contact of Pt electrode), but was always almost two orders of magnitude smaller than the large arc and neglected in the analysis. The absence of a pronounced grain boundary related arc indicates that charge transport is not severely hindered by grain boundaries. We interpret the resistance of the main arc as the bulk resistance which is also in accordance with its capacitance, see below. However, effects of highly conductive grain boundaries cannot be excluded by such macroscopic impedance measurements, but would require local conductivity data, cf. Ref. [34]. For calculation of the PZT bulk resistance and capacitance, the spectra (without low frequency "artifact") were fitted to a parallel connection of a resistor R and a constant phase element (CPE) with impedance

$$Z = \frac{1}{(i\omega)^n Q} \tag{1}$$

Symbols n and Q denote the fitting parameters and were used to calculate the sample capacitance [35] according to

$$C = \left(R^{1-n}Q\right)^{1/n} \tag{2}$$

A typical fit curve is shown in Fig. 1b. The n-values were in general above 0.93 and the CPE thus reflects a rather ideal capacitance. Alternatively, an ideal capacitor instead of the CPE was used in the fit for determination of the capacitance. From the PZT resistances and capacitances conductivities and the sample permittivity was calculated.

Figure 2 shows the conductivity change during first equilibration and the first conductivity relaxation measurement after a partial pressure step from air to pure oxygen at 611 °C. When exposing the as-prepared PZT samples for the first time to air at elevated temperatures, conductivity changes took place on a time scale much larger than that found in subsequent conductivity relaxation experiments after pO_2 steps: A comparatively fast change was followed by slight further changes. Despite unknown nature of these additional changes (possibly cation related effects) this first equilibration was completed before systematic oxygen partial pressure steps were started.

Figure 2 also displays that the conductivity changes significantly when alternating the oxygen partial pressure, while the relative permittivity remained almost constant both during first equilibration and subsequent pO_2 changes (Fig. 2b and c). The CPE fit is more accurate in terms of the resistance but shows more scattered permittivity data (Fig. 2b) than the ideal capacitor approximation (n=1, Fig. 2c). However, permittivity values are very similar in both cases (relative permittivity between 800 and 850 at 611 °C) and correspond to values typical for PZT at such temperatures [26, 36].

A measurement cycle consisted of numerous oxygen partial pressure changes, partly with duration of several weeks. During such a cycle, a long time drift of the conductivity is observed (Fig. 3). Since this drift is found to be many orders of magnitude slower than chemical oxygen diffusion (resulting from oxygen partial pressure changes) we suppose changes of the cation lattice to be responsible. Even though this slight drift was much smaller than the conductivity changes after an oxygen partial pressure step, a correction of the conductivities to the time t^* after the first pO_2 step (to 100 % oxygen) was performed. Accordingly measured conductivities σ

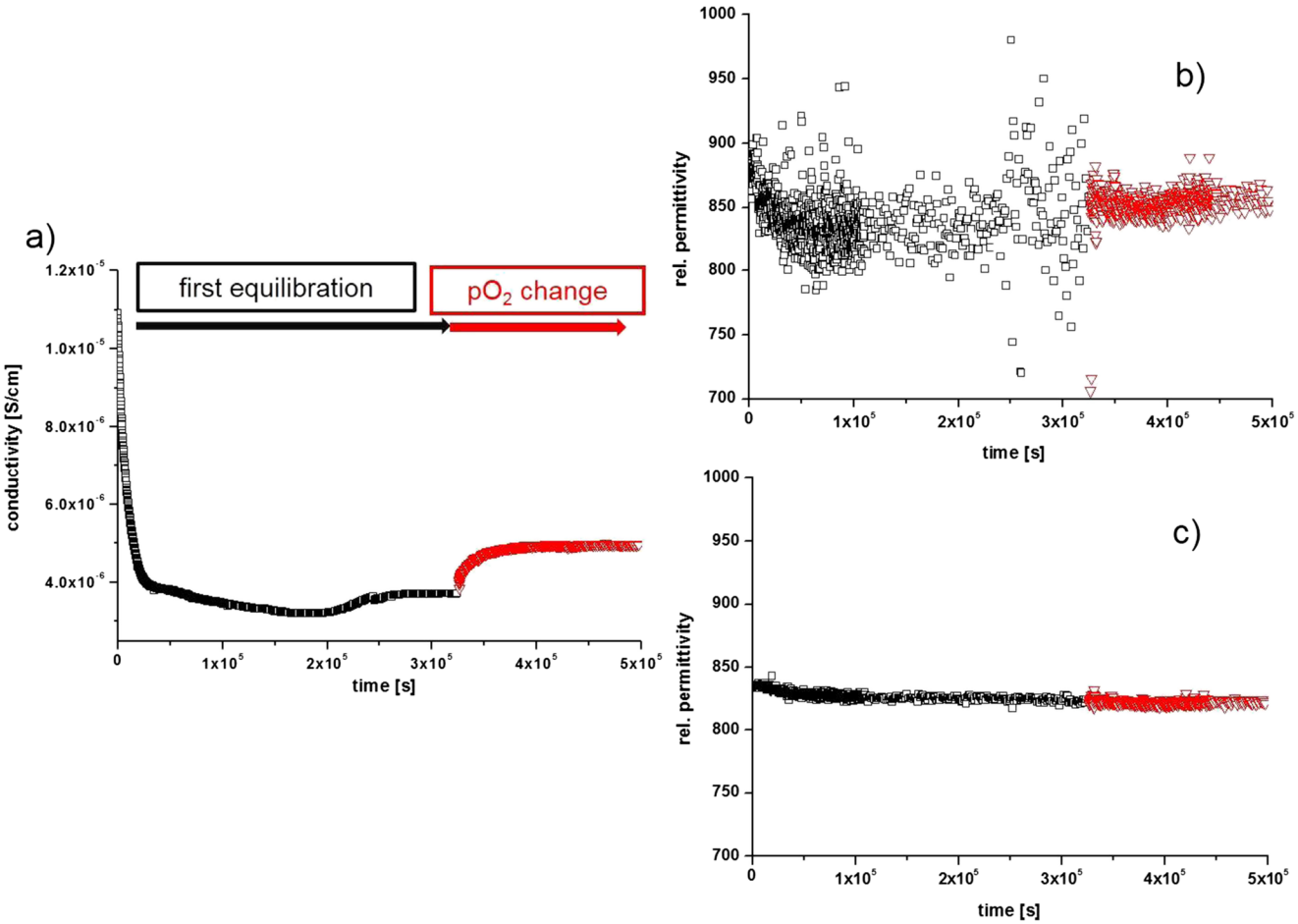

Fig. 2 Conductivity and relative permittivity at 611 °C vs. time during first equilibration in air (open squares) and for the first oxygen partial pressure step to 100 % oxygen (filled triangles). **a** Conductivity vs. time, **b** permittivity for capacitances calculated from a fit using a CPE element and Eq. 2, **c** permittivity calculated from a fit using an ideal capacitance

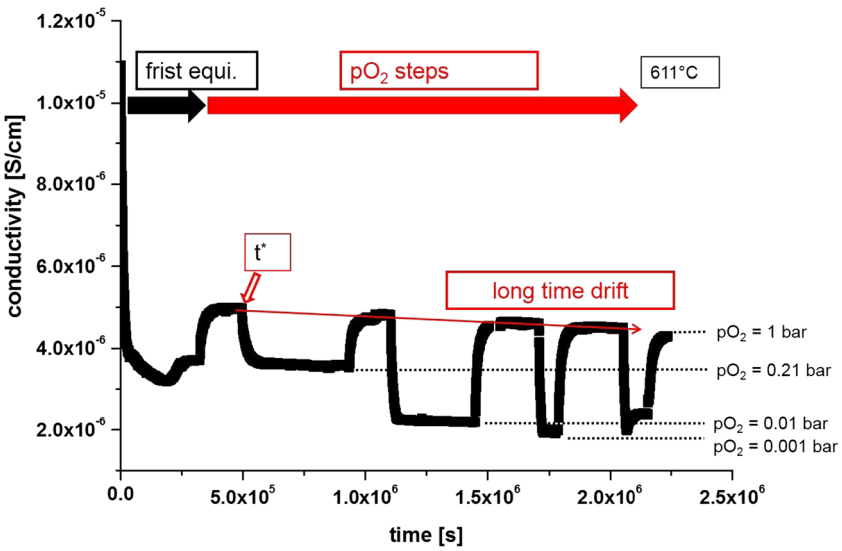

Fig. 3 Conductivity vs. time during first equilibration and various oxygen partial pressure steps at 611 °C. The measurement also reveals a long time drift; t^* indicates the time to which conductivity values were corrected (σ^*)

(obtained Δt after t^*) were recalculated to σ^* values according to

$$\sigma^* = \frac{\sigma}{1 + f_c \Delta t} \quad (3)$$

with f_c being the relative conductivity change per time extrapolated from the slope of the measurements in pure oxygen, cf. line in Fig. 3

It is known that PZT is thermodynamically unstable under very reducing conditions such as the pO_2 of ca $2 \cdot 10^{-25}$ bar established by 2.5 % H_2 in humidified Ar. However, a certain meta-stability of PZT might still reveal additional information on the defect chemical situation. Hence, steps to H_2-containing atmosphere were performed for several samples and a typical time dependence measured after a gas change from pure nitrogen to humidified hydrogen is given in Fig. 4. After a short decrease of the conductivity, a strong increase is observed, which is much faster than any change found between higher pO_2 values. (Please note the logarithmic time scale in Fig. 4.) After the very fast initial change, a slow but continuous further conductivity increase is found which did not come to an end for any of the samples investigated. In the quantitative data analysis of section 3.2, a conductivity value close to the beginning of the slow conductivity increase is used (see arrow in Fig. 4). A gas exchange back to pO_2=1 bar lead to a very slow regeneration of the conductivity to values common for such pressures (Fig. 4). However, the value measured for pO_2=1 bar before exposure to hydrogen was not reached (not shown here). This might indicate formation of a second phase on a longer time scale in H_2. A more detailed analysis of the processes during H_2 exposure is beyond the scope of this paper. Different mechanisms of hydrogen induced changes of PZT are discussed in literature: among others incorporation of hydrogen forming hydroxide ions was supposed to be responsible for changes in the material [37, 38] and also lead formation was observed for PZT samples accompanied by significant optical and resistive changes [39].

3.2 Partial pressure dependence of the conductivity and conduction mechanism in donor-doped PZT

The corrected equilibrium conductivity σ^* extracted from the conductivity vs. time measurements (e.g. Fig. 3) can now be plotted versus the oxygen partial pressure. Figure 5 shows the plots for 611 °C, 565 °C and 560 °C. All curves clearly show a positive slope close to 0.25 at high oxygen partial pressures, which already strongly suggests predominant hole conduction in this pO_2 range [40]. Accordingly, the onset of a negative slope for low pO_2 indicates electron conduction under more reducing conditions. Such a behavior is in clear contrast to donor-doped STO or BTO, where at least at high temperatures (> 1000 °C) the conductivity is dominated by electron conduction with a plateau or a negative slope in the entire pO_2 range, depending on dopant level and temperature [6, 41]. For the moderate temperatures used in our study, donor-doped BTO and STO show such a slow equilibration kinetics, that equilibrium conductivities are not available.

Rather, the behavior shown in Fig. 5 is known for undoped or slightly acceptor-doped perovskites [6, 7, 10, 12, 14]. Also the conductivity of acceptor-doped PZT published for temperatures ranging from 500 to 700 °C exhibit a slope of approx. 0.25 (getting smaller with decreasing temperature) in the pO_2 range of 1 to 10^{-4} bar [20]. However, in contrast to acceptor-doped STO [14] a plateau region between the supposedly electron and hole conducting regimes, indicating ion conduction, is not found in our case. Therefore we further analyzed the data based on the assumption of negligible oxygen ionic conductivity. Assuming a power law behavior

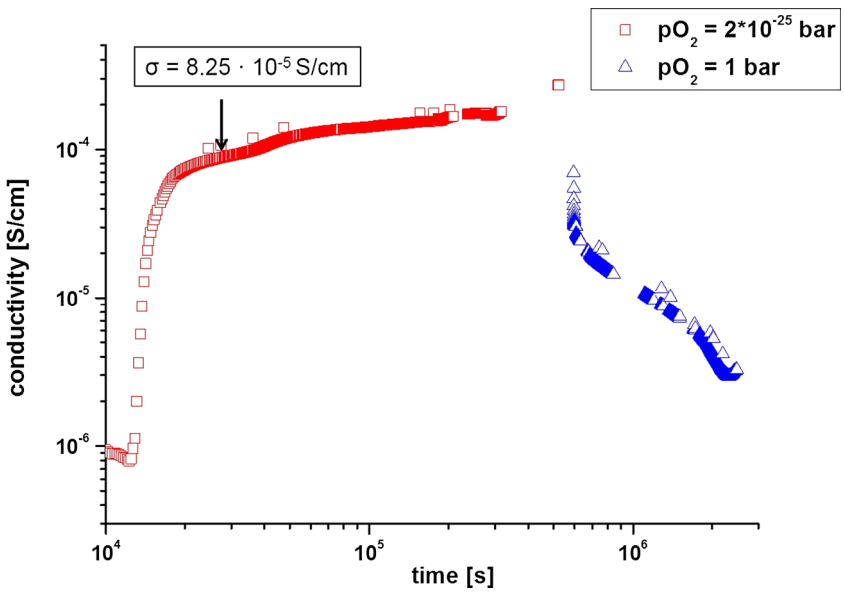

Fig. 4 Corrected conductivity for oxygen partial pressure step from pure nitrogen to humidified H_2 (2.5 % H_2 in Ar, humidified at room temperature, i.e. ca. $2 \cdot 10^{-25}$ bar oxygen partial pressure) at 565 °C followed by a step to 100 % O_2. After the first strong increase of the conductivity in hydrogen, a slow but continuous change occurs. The impedance spectra of the final material do not show a complete arc in the complex impedance plane, but a low frequency resistance of ca. 400 Ohm. After switching back to oxygen the sample only recovers very slowly (logarithmical time scale!). The whole measurement took 14 days

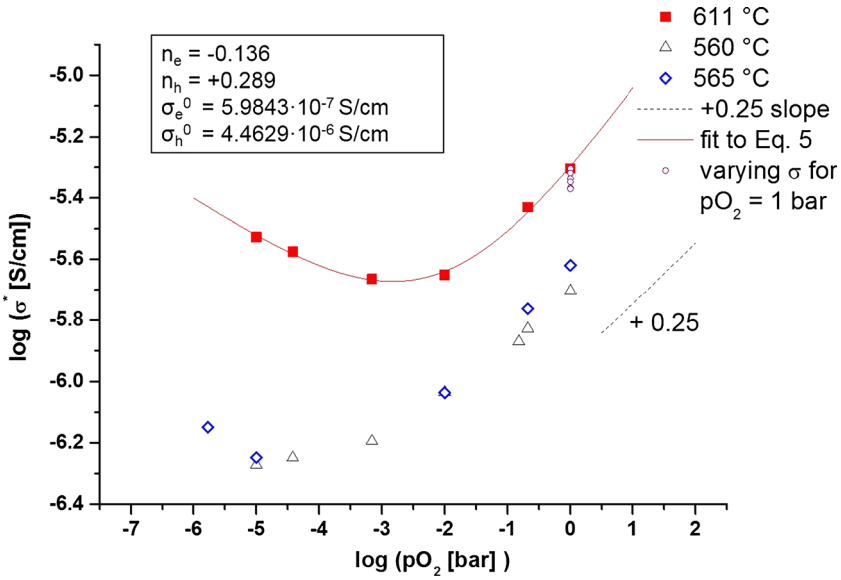

Fig. 5 Conductivity vs. oxygen partial pressure measured at 611 °C, 565 °C and 560 °C with fit line according to Eq. 5 for 611 °C. The open circles represent the true conductivity values in pure oxygen during the long time drift (before correction by Eq. 3)

of hole as well as electron conduction [31], the following expressions for the entire electronic conductivity as a function of the unitless partial pressure p_{O2} results:

$$\sigma = \sigma_e^0 p_{O_2}^{n_e} + \sigma_h^0 p_{O_2}^{n_h} \tag{4}$$

$$\log\sigma = \log\left(\sigma_e^0 10^{n_e \log(pO_2)} + \sigma_h^0 10^{n_h \log(pO_2)}\right) \tag{5}$$

The logarithmic version (Eq. 5) was used in a nonlinear least square fit to determine the slopes n_e and n_h and σ_e^0 as well as σ_h^0, which are the hole and electron conductivity at 1 bar, respectively. The resulting fit for 611 °C is presented in Fig. 5. Hole conduction exhibits a slope of +0.289, electron conduction of −0.136 at 611 °C. At 1 bar the corresponding hole conductivity exceeds the electron conductivity by a factor of 7. Figure 5 also displays the drift of the uncorrected conductivity values for 100 % oxygen.

The slope n_h=0.289 is close to the value of +1/4, expected in the hole conducting regime of an acceptor doped material (see also below). Nd^{3+} donor doping of PZT, on the other hand, should be compensated by lead vacancies or electrons, depending on the oxygen partial pressure. At first glance, one might therefore expect hole conduction to be completely suppressed in the oxygen partial pressure range under investigation. However, here the high volatility of PbO comes into play. Our results strongly suggest that the additional defects formed in PZT by PbO evaporation during sintering change the material into effectively acceptor-doped PZT, at least in the temperature range considered here. More quantitatively: in the most simple case of donor-doped materials, the donor concentration $[D^{\bullet}]$ is completely counter-balanced by the formation of lead vacancies with their concentration $\left[V_{Pb}''\right]$ being half the donor concentration. At sintering temperatures, the PbO volatility increases the lead vacancy concentration of PZT above the level of ½ $[D^{\bullet}]$ and the charge neutrality equation has to include further charge carriers and reads (without trapping effects)

$$[h^{\bullet}] + 2\left[V_o^{\bullet\bullet}\right] + [D^{\bullet}] = 2\left[V_{Pb}''\right] + \left[e'\right] \tag{6}$$

Donor and cation vacancy concentrations become frozen-in at temperatures much below the sintering temperature and only the electron $[e']$, electron hole $[h^{\bullet}]$ and oxygen vacancy $\left[V_o^{\bullet\bullet}\right]$ concentrations remain variable. Lead vacancies are then acceptor-type and the high lead vacancy level (caused by PbO evaporation) turns the material into effectively acceptor-doped PZT with effective acceptor concentration

$$\left[A_{eff}'\right] = 2\left[V_{Pb}''\right] - [D^{\bullet}] \tag{7}$$

Accordingly, in terms of electronic charge carriers and oxygen vacancies such a material behaves like slightly acceptor-doped PZT and at higher oxygen partial pressures, A'_{eff} is either compensated by holes or oxygen vacancies. The oxygen exchange equilibrium.

$$^1/_2 O_2 + V_O^{\bullet\bullet} \leftrightarrow O_o^x + 2h^{\bullet} \tag{8}$$

with mass action law (K_p being the mass action constant)

$$\frac{[h^{\bullet}]^2}{V_O^{\bullet\bullet}} = K_p\, pO_2^{1/2} \tag{9}$$

and predominant oxygen vacancy compensation of the effective acceptors, i.e. $\left[V_o^{\bullet\bullet}\right]$ =½ $[A'_{eff}]$, leads to a +1/4 slope of the

hole conduction in the log (σ)-log (pO_2) plot. This is almost exactly what we found and hence we conclude that our nominally donor-doped PZT is indeed hole conducting in the high pO_2 regime. This is also in accordance with earlier indication of hole conduction in nominally donor-doped PZT [25, 29].

All trends observed at 611 °C could be reproduced in (time-consuming) measurements for two samples at 560 and 565 °C, see Fig. 5. Again a positive slope for higher pO_2 close to+¼ is found but the minimum conductivity with transition to electron conduction is shifted to lower pressures and pure electron conduction is hardly visible. This shift of the minimum is again in accordance with data found for acceptor-doped STO [2, 14] and supports our interpretation. However, still the slope of -0.14 found at 611 °C for lower pO_2 deserves some discussion. Inserting the mass action law of electronic band-band equilibrium $[e^{/}]\cdot[h^{\bullet}]=K_e$ into Eq. 9 would lead to a slope of -1/4 for the electron conductivity. The measured smaller slope may simply be an artifact due to few data points in the electron conducting regime.

However, a slope of -1/6 can indeed be expected for effectively undoped material with the charge neutrality being given by $[e^{/}]=2\left[V_o^{\bullet\bullet}\right]$. Such a defect chemical situation is not unrealistic in our case, at least at even lower pO_2 since the effective acceptor concentration $[A^{/}_{eff}]$ might be very low - it reflects the surplus of lead vacancies compared to the donor level (Eq. 7), introduced by lead oxide evaporation during sintering. This surplus and thus also the dopant induced oxygen vacancy levels might be small. A low oxygen vacancy concentration (and thus a low acceptor level) is also indicated by the absence of an ion conduction plateau between electron and hole conducting regimes. Moreover, analysis of ^{18}O tracer diffusion profiles with space charge effects on similarly prepared PZT [42] and impedance measurements using ion-blocking electrodes (publication in preparation) suggest a low oxygen vacancy concentration in the ppm range. In such a case a -1/6 slope is expected already for moderately low pO_2. In order to check the validity of this hypothesis we also performed the measurements in hydrogen, despite stability problems, see Section 3.1. Figure 6 displays the data for 565 °C and the conductivity value determined in H_2 is indeed in reasonable agreement with a -1/6 slope model. Accordingly, at least for very low pO_2 our effectively acceptor-doped PZT seems to reach a defect chemical regime in which electron and hole concentrations are unaffected by dopants, but only depend on the mass action law constants K_p and K_e. In Fig. 6 we also indicate the conductivity found in pure O_2 after the exposure to H_2 (cf. Fig. 4). The value is slightly enhanced, possibly due to formation of additional lead vacancies during H_2 exposure and thus increase of the effective acceptor concentration according to Eq. 7 (cf. formation of pure lead under such conditions Ref. [39]). In summary, we conclude from all conductivity data that also in nominally donor-doped PZT a small but still relevant oxygen vacancy concentration is present and that (in contrast to donor-doped BTO and STO) the material is effectively acceptor-doped, at least from a conductivity point of view. This interpretation is also in accordance with the decrease of bulk conductivity by donor doping discussed in Ref. [21].

3.3 Chemical diffusion coefficient of oxygen

When altering an equilibrated sample at a fixed temperature from a partial pressure P_1 to a final partial pressure P_2 it is possible to extract the chemical diffusion coefficient of oxygen from the time dependence of the conductivity [31, 43]. Figure 7 shows the relaxation behavior of PZT at 560 °C after an oxygen partial pressure step from air to 1 % oxygen. Oxygen exchange between the sample and the gas phase and thus relaxation of the conductivity takes place within some hours depending on the partial pressure and temperature. Owing to the large aspect ratio of the samples used in this study (see Fig. 1) equilibration mainly occurs via the large top and bottom sides and to a good approximation diffusion can be considered one dimensional. For such a one dimensional diffusion from two sides of a sample with thickness L, the long-time behavior of the mean sample conductivity σ_m (t) can be expressed by [31, 43]

$$\frac{\sigma_m(t)-\sigma_1}{\sigma_2-\sigma_1}=1-\frac{8}{\pi^2}\exp\left(-\frac{t}{\tau}\right) \tag{10}$$

$$\ln\left(1-\frac{\sigma_m(t)-\sigma_1}{\sigma_2-\sigma_1}\right)=\ln\left(\frac{8}{\pi^2}\right)-\frac{t}{\tau};\tau=\frac{L^2}{\pi^2 D^{\delta}} \tag{11}$$

In Eqs. 12 and 13 σ_1 and σ_2 denote the equilibrium conductivities for partial pressures P_1 and P_2 and the time constant τ can be used to extract the chemical diffusion coefficient D^{δ}, provided the oxygen surface exchange is sufficiently fast and does not play a role on the given time scale. From oxygen tracer diffusion studies on these and very similar materials we found critical lengths to be several orders of magnitude shorter than our sample thickness.[15, 44]. Despite differences between tracer diffusion and chemical diffusion we therefore conclude validity of diffusion limitation also in these experiments. In Fig. 7 it is shown that Eq. 11 indeed fits to our results: after an initial sharp decay (not analyzed) the logarithmic plot of the normalized conductivity (Eq. 10) shows a linear behavior. The slope of the resulting linear fit reveals D^{δ} according to Eq. 11. The values of D^{δ} are approximately $6.5\cdot10^{-9}$ cm^2/s at 560 °C and $2.0\cdot10^{-8}$ cm^2/s at 611 °C when switching between different pressures in

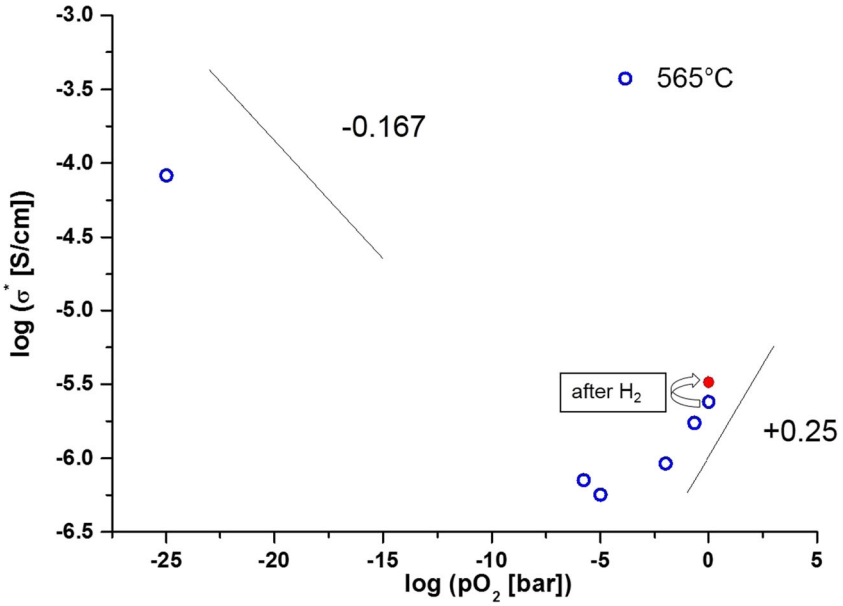

Fig. 6 Corrected conductivity vs. oxygen partial pressure measured at 565 °C with conductivity value for H_2 exposition. Data suggest a slope of ca.−1/6 for electron conduction (slopes of−1/6 and + 1/4 are indicated by solid lines). The filled circle represents the uncorrected conductivity at pO_2= 1 bar after the H_2 exposure and very long annealing in oxygen

the hole conducting regime – a systematic pO_2 dependence could not be obtained in this range. Ref. [18] reports a much higher value of about $2.0\cdot10^{-4}$ cm^2/s at 700 °C in air for 0.75 % Nb doped PZT, but in that case impedance data indicated much higher ionic conductivity. In general, the chemical diffusion coefficient of a material with oxygen vacancy diffusion coefficient D_V and hole diffusion coefficient D_h reads [31]

$$D^{\delta} = \frac{F^2}{RT}\frac{D_V D_h}{\sigma}\left([h^{\bullet}] + 4\left[V_o^{\bullet\bullet}\right]\right) \tag{12}$$

Symbols F and T denote Faraday's constant and temperature, respectively. In section 3.2 we showed that our PZT is predominantly hole conducting in the partial pressure regime considered here with $\left[V_o^{\bullet\bullet}\right]$ >>[h·]. For such a vacancy rich hole conductor the chemical diffusion coefficient in Eq. 12 can be reduced to [31]

$$D^{\delta} = \frac{4\left[V_o^{\bullet\bullet}\right]}{[h^{\bullet}]}D_V \tag{13}$$

Therefore we conclude that in our study the oxygen vacancy concentration (and thus the effective acceptor doping level) was much lower than in Ref. [18], most probably due to less lead oxide evaporation and thus less additional lead vacancy formation during sintering or pre-annealing. In Ref. [26], a high chemical diffusion coefficient of about $2.3\cdot10^{-7}$ cm^2/s was found for undoped PZT at 360 °C, but those samples showed high ionic conductivity as well. It is finally worth mentioning that hole trapping would add an additional factor to Eq. 13, cf. Ref. [31], and thus even a known D_V value

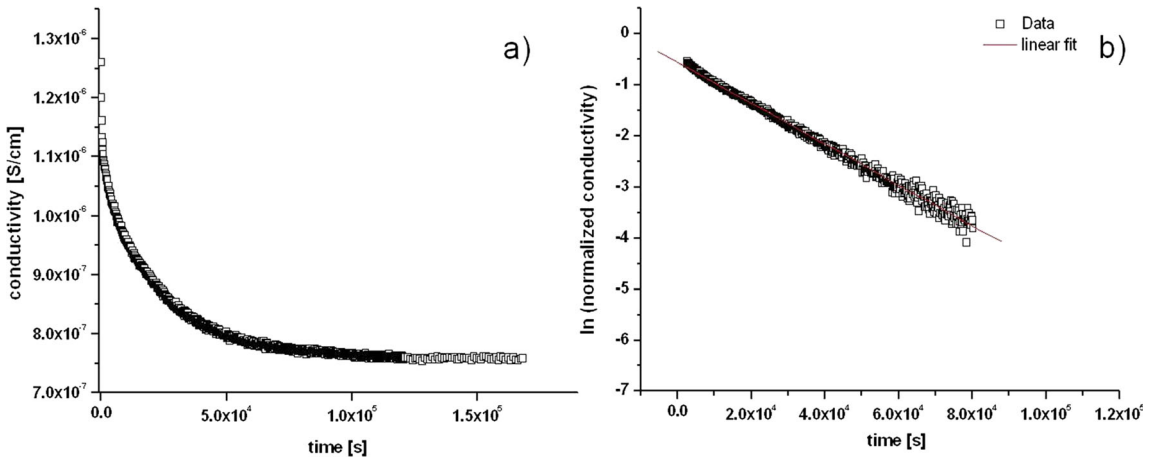

Fig. 7 Conductivity data for an oxygen partial pressure step from ambient air to 1 % oxygen at 560 °C in a linear **a** and logarithmic **b** plot including the fit line according to Eq. 11

would not allow a quantitative determination of $\left[V_o^{\bullet\bullet}\right]$ /[h·] from the measured diffusion coefficients.

4 Conclusions

Conductivity studies were performed on donor-doped PZT in order to obtain defect chemical information and to identify the relevant mobile charge carriers. From time, temperature and partial pressure dependent measurements the following main results could be deduced:

- Oxygen partial pressure steps are reversible in a certain partial pressure range and allow analysis of diffusion coefficients and equilibrium conductivities. For very low oxygen partial pressures (H_2 exposition), irreversible changes of the material are observed.
- At higher oxygen partial pressures, the slopes of log (conductivity) vs. log (pO_2) plots (~1/4) clearly indicate hole conduction, despite nominal donor doping. This can be explained by PbO evaporation during preparation. The additionally formed lead vacancies turn the nominally donor-doped PZT into an effectively slightly acceptor-doped oxide.
- A transition to electron conduction is found for lower pO_2 and this transition is shifted to lower pressures at lower temperatures. Moreover, a decreased slope (less than−¼) in this regime indicates a very low effective acceptor doping.
- Conductivity relaxation measurements after pO_2 steps also allow analysis of the chemical diffusion coefficient of oxygen and values of about $6.5\cdot10^{-9}$ cm^2/s and $2\cdot10^{-8}$ cm^2/s were determined for 560 and 611 °C, respectively. Comparison to literature values suggests low oxygen vacancy concentration in our case, in accordance with the reduced slope of the conductivity data for low partial pressures and the absence of a conductivity plateau.

Acknowledgement Financial support by Christian Doppler Research Association (CDG) is gratefully acknowledged.

References

1. J. Daniels, K.H. Härdtl, R. Wernicke, Philips Technol. Rev **38**, 73–82 (1978)
2. J. Gerblinger, H. Meixner, Sensors Actuators B Chem. **4**, 99–102 (1991)
3. W. Heywang, K. Lubitz, W. Wersing, Piezoelectricity, Evolution and Future of a Technology, (2008)
4. G.H. Haertling, J. Am. Ceram. Soc. **82**, 797–818 (1999)
5. R. Waser, T. Baiatu, K.H. Härdtl, J. Am. Soc. **73**(6), 1654–1662 (1990)
6. J. Daniels, K.H. Härdtl, Philips Res. Repts. **31**, 489–504 (1976)
7. J. Daniels, K.H. Härdtl, R. Wernicke, Philips Technol. Rev **38**, 73–82 (1976)
8. N.H. Chan, R.K. Sharma, D.M. Smyth, J. Am. Ceram. Soc. **64**, 556–562 (1981)
9. H. Neumann, G. Arlt, Ferroelectrics **69**(1), 179–186 (1986)
10. H.L. Tuller, Solid State Ionics **94**, 63–74 (1997)
11. R. Moos, K.H. Hardtl, J. Am. Ceram. Soc. **80**, 2549–2562 (1997)
12. I. Denk, W. Münch, J. Maier, J. Am. Ceram. Soc. **78**, 3265–3272 (1995)
13. S. Rodewald, J. Fleig, J. Maier, J. Am. Ceram. Soc. **83**, 1969–1976 (2000)
14. S. Steinsvik, R. Bugge, J.O.N. GjoeNnes, J. Taftoe, T. Norby, J. Phys. Chem. Solids **58**, 969–976 (1997)
15. T. Frömling, A. Schintlmeister, H. Hutter, J. Fleig, J. Am. Ceram. Soc. **94**, 1173–1181 (2011)
16. M.V. Raymond, D.M. Smyth, Ferroelectrics **144**, 129–135 (1993)
17. M.V. Raymond, D.M. Smyth, J. Phys. Chem. Solids **57**, 1507–1511 (1996)
18. N.J. Donnelly, C.A. Randall, Applied Physics Letters **96** (2010) 052906-052906-052903.
19. L. Andrejs, J. Fleig, J. Eur. Ceram. Soc. **33**, 779–794 (2013)
20. M.V. Raymond, D.M. Smyth, Integr. Ferroelectr. **4**, 145–154 (1994)
21. Y. Xu, X. Yuhuan, Ferroelectric materials and their applications, North-Holland Amsterdam ets, (1991)
22. J. Maier, Phys. Chem. Chem. Phys. **5**, 2164–2173 (2003)
23. D.L. Corker, R.W. Whatmore, E. Ringgaard, W.W. Wolny, J. Eur. Ceram. Soc. **20**, 2039–2045 (2000)
24. A.J. Moulson, J.M. Herbert, Electroceramics, John Wiley & Sons, Ltd, (2003)
25. N.J. Donnelly, C.A. Randall, J. Appl. Phys. **109**, 104107–104106 (2011)
26. B.A. Boukamp, M.T.N. Pham, D.H.A. Blank, H.J.M. Bouwmeester, Solid State Ionics **170**, 239–254 (2004)
27. D.M. Smyth, Curr. Opinion Solid State Mater. Sci. **1**, 692–697 (1996)
28. J.v. Rudolph, Zeitschrift Naturforschung Teil A **14** (1959) 727.
29. B. Jaffe, W.R. Cook, H. Jaffe, Piezoelectric Ceramics, Academic Press London and New York, (1971)
30. W. Long, W. Tien-Shou, W. Chung-Chuang, L. Hsi-Chuan, J. Phys. C Solid State Phys. **16**, 2823 (1983)
31. J. Maier, Physical Chemistry of Ionic Materials, John Wiley & Sons, Ltd, (2005)
32. J. Jamnik, J. Maier, Phys. Chem. Chem. Phys. **3**, 1668–1678 (2001)
33. J. Jamnik, J. Maier, J. Electrochem. Soc. **146**(11), 4183–4188 (1999)
34. J. Fleig, J. Maier, Phys. Chem. Chem. Phys. **1**, 3315–3320 (1999)
35. J. Fleig, Solid State Ionics **150**, 181–193 (2002)
36. D. Fasquelle, J.C. Carru, J. Eur. Ceram. Soc. **28**, 2071–2074 (2008)
37. A. Shafiei, C. Oprea, A. Alfantazi, T. Troczynski, J. Appl. Phys. **109**, 114108 (2011)
38. M. Wu, H. Huang, B. Jiang, W. Chu, Y. Su, J. Li, L. Qiao, J. Mater. Sci. **44**, 5768–5772 (2009)
39. Y. Shimakawa, Y. Kubo, Appl. Phys. Lett. **77**, 2590–2592 (2000)
40. Y.-M. Chiang, D.P. Birnie, W.D. Kingery, Physical ceramics, J. Wiley, (1997)
41. R. Moos, W. Menesklou, K.H. Härdtl, Appl. Phys. A **61**, 389–395 (1995)
42. T. Frömling, H. Hutter, J. Fleig, J. Am. Ceram. Soc. **95**, 1692–1700 (2012)
43. W. Preis, E. Bucher, W. Sitte, Solid State Ionics **175**, 393–397 (2004)
44. G. Holzlechner, D. Kastner, C. Slouka, H. Hutter, J. Fleig, Solid State Ionics **262**, 625–629 (2014)